RSC Advances

PAPER

View Article Online
View Journal | View Issue

Cite this: *RSC Adv.*, 2025, **15**, 17781

Galactose-modified erythrocyte membrane fusion liposomes enable the targeted delivery of drug nanoparticles to the liver

Jiayu Song,[bc] Huanhuan Zhang,[b] Xiaohui Zhang,[b] Meiying Liu,[b] Dan Peng,[b] Yuan Ren,[b] Yan Sun[b] and Yunlan Li *[ab]

Received 19th October 2024
Accepted 11th April 2025

DOI: 10.1039/d4ra07489k

rsc.li/rsc-advances

The safe and efficient delivery of chemicals and biologics remains crucial for liver disease therapy. In this study, we developed a targeted drug delivery system utilizing a galactose-modified erythrocyte membrane coating technique and drug liposome nanoparticles, which were further optimized using orthogonal experiments and response surface analysis. The specificity, precision, accuracy, and stability exhibited satisfactory performance in bioanalytical analysis. Specifically, targeting ligands (Gal-DSPE-PEG3400) were efficiently inserted into red blood cell (RBC) membranes using a facile insertion method. When Gal-DSPE-PEG3400-RBC was fused with fenofibrate liposome nanoparticles (FNB-Lip) by co-extrusion, the resulting galactose-modified erythrocyte membrane fusion liposome nanoparticles (Gal-RBC-FNB-Lip) showed long-term stability, excellent biocompatibility, prolonged retention time, and superior liver accumulation and therapeutic efficacy. These qualities make it suitable for effective drug delivery. The findings of this study will provide a fundamental basis for research and development of liver-targeted drugs and offer novel insights into the treatment of clinical liver diseases.

1. Introduction

According to the 2023 Global Burden of Disease Project, more than 2 million people died from major liver diseases, including alcohol-related liver disease, non-alcoholic fatty liver disease, acute hepatitis, cirrhosis and liver cancer, accounting for approximately 4% of global mortality (equivalent to 1 in every 25 deaths worldwide).[1] In recent years, numerous clinical studies on liver disease have been conducted globally; however, no efficacious treatment has been discovered.[2,3] With the contemporary focus on precision medicine, the precise administration of pharmaceutical agents is being increasingly recognized as an innovative treatment approach.[4,5] Numerous studies have shown that precision-targeted delivery enhances drug pharmacokinetics, mitigates toxic side effects, and promotes patient adherence.[6–8] Moreover, it facilitates the clinical application of chemicals and biologics that were previously deemed impractical due to toxicity, rapid clearance, or off-target deposition.[9]

Currently, there is a growing body of research focusing on liver-targeted systems, with particular significance attributed to the sialic acid glycoprotein receptor (ASGPR).[10–13] ASGPR, also known as the galactose receptor, exhibits specific recognition and binding capabilities towards galactose residues.[14] Its primary role involves the regulation of galactose-like coagulation factors, as well as the recognition, binding, internalization, and elimination of compounds containing galactose residues from the bloodstream.[14–16] Due to the exclusive presence of ASGPR in the cell membrane receptor of liver parenchyma, the specific binding characteristics between galactose and ASGPR enable the development of liver-targeted drugs,[17] thereby minimizing potential adverse effects on other tissues and organs.

In a targeted drug delivery system, the drug carrier plays a crucial role in determining the drug loading capacity, release rate, and biological compatibility.[18,19] Liposomes are composed of single or multi-layered enclosed vesicles, featuring a phospholipid bilayer structure that closely resemble the cellular biofilm structure, thereby exhibiting strong affinity.[20] The bilayer structure of liposomes confers inherent advantages, enabling the encapsulation of polar drugs within the hydrophilic core and lipid drugs within the hydrophobic shell.[21] Moreover, liposomes exhibit biocompatibility, natural targeting ability, low toxicity, and structural modifiability, among other merits.[22] Consequently, numerous drugs in liposomal formulations have been successfully commercialized. Furthermore, extensive investigations have also been conducted on endogenous biological carriers, such as red blood cells (RBCs), macrophages, stem cells, and tumor cells.[23] RBCs, lacking a nucleus, are considered innate immune cells that possess a unique advantage due to their intrinsic biocompatible

[a]School of Public Health, Shaanxi University of Chinese Medicine, Xi'an, 712046, P. R. China
[b]School of Pharmaceutical Science, Shanxi Medical University, Taiyuan, 030001, P. R. China. E-mail: liyunlanrr@163.com; Tel: +86 13111066649
[c]College of Medical Technology, Luohe Medical College, Luohe, 462000, P. R. China

membrane compared to conventional carrier systems.[24] Consequently, the utilization of RBCs as drug delivery vehicles circumvents potential issues like blood agglutination or rejection and effectively extends the drug's half-life.[25]

Fenofibrate (FNB), a derivative of clofibrate, exhibits lipid-regulating properties;[26] however, it demonstrates limited aqueous solubility at only 0.3 μg mL^{-1}, classifying it as a BCS class II drug with high lipophilicity and low bioavailability.[27] In this study, we successfully synthesized galactose-modified red blood cell membrane-fused FNB liposomes. Subsequently, both *in vivo* and *in vitro* experiments were conducted to investigate their hepatic targeting ability. The findings of this study will provide a fundamental basis for the research and development of liver-targeted drugs and offer novel insights into the treatment of clinical liver diseases.

2. Material and methods

2.1 Material

The methanol (20210331) was obtained from Comiou Chemical Reagent Co., Ltd (Tianjin, China). Galactosamine hydrochloride (L1905043), triethylamine (I12018168), Cremophor EL (11916053), DSPE PEG3400-NHS (K2103306), *N*,*N*-dimethylformamide (J2022250), lecithin (A1909011), cholesterol (H1926053), fenofibrate (FNB) (A1915135), rhodamine B (RhB) dye (B2102172), and indocyanine green dye (ICG) were all purchased from Aladdin Biochemical Technology Co., Ltd (Shanghai China). Fetal bovine serum (FBS) (1925624) was acquired from Cellmax Cell Technology Co., Ltd. Dimethyl sulfoxide (DMSO) (710N033), penicillin–streptomycin mixture (20190525), and MTT (715F053) were obtained from Soleibao Technology Co., Ltd. 0.25% trypsin solution (MA0232) and DMEM high glucose medium (GP21070153107) were both sourced from Boster Biotechnology Co., Ltd in Wuhan, China. Total cholesterol (TC) (20211203) and triglyceride (TG) kit (20211206) were acquired from Nanjing Jiancheng Bioengineering Research Institute (Nanjing, China). DiI (C1036) and DiD (C1039) were purchased from Shanghai Beyotime Biotechnology Co.

2.1.1 Cells. The normal hepatocyte cell line (HL-02) was obtained from Wuhan Boster Biological Engineering Co., Ltd (Wuhan, PR China). The cells were cultured in DMEM supplemented with 10% FBS and 1% penicillin/streptomycin and maintained under standard conditions (37 °C, 5% CO_2) in a cell culture incubator.

2.2 Orthogonal design and optimization of fenofibrate liposome nanoparticles (FNB-Lip)

The concentrations of phospholipids (A), the phospholipid–cholesterol ratio(B), and the phospholipid–drug ratio (C) were considered as independent variables, with four levels assigned for each variable (Table 1). To optimize the preparation conditions of FNB-Lip, a L16(4^3) orthogonal table was employed as shown in (Table 2), considering encapsulation efficiency (EE) and drug loading (DL) as our investigation indices. After weighing the phospholipids, cholesterol, and FNB, 20 mL of methanol was added. Subsequently, the solution underwent dissolution through ultrasound treatment before being evaporated under reduced pressure for 2 h to generate lipid films. Then, hydration was accomplished by adding 10 mL of PBS for 30 min, leading to liposome formation. Once hydration was completed, the liposomes were transferred into an EP tube and subjected to sonication at 240 W for 30 min until the bulk lipid was disrupted, yielding the liposome suspension. Liposome suspension was then extruded using a liposome extruder to obtain FNB-Lip, followed by an analysis of the differences in EE and DL. Consequently, the key factors influencing the EE and DL of FNB-Lip were determined. Additionally, the response surface methodology was employed to optimize the preparation conditions of FNB-Lip through a three-factor, three-level experiment using Design-Expert 12.

Table 1 Level of factors

	Factors		
Levels	*A*	*B*	*C*
1	20	2 : 1	3 : 1
2	30	3 : 1	5 : 1
3	40	4 : 1	6 : 1
4	50	5 : 1	8 : 1

Table 2 Orthogonal test

	Levels		
Orthogonality	*A*	*B*	*C*
1	30	5 : 1	8 : 1
2	30	3 : 1	6 : 1
3	50	5 : 1	6 : 1
4	40	2 : 1	8 : 1
5	40	4 : 1	6 : 1
6	20	5 : 1	5 : 1
7	20	2 : 1	6 : 1
8	20	3 : 1	3 : 1
9	40	5 : 1	3 : 1
10	20	4 : 1	8 : 1
11	50	3 : 1	8 : 1
12	50	4 : 1	3 : 1
13	30	2 : 1	3 : 1
14	40	3 : 1	5 : 1
15	50	2 : 1	5 : 1
16	30	4 : 1	5 : 1

2.3 Determination of EE and DL

The liposome solution and the supernatant obtained after centrifugation at 14 000 rpm for 30 min, were individually diluted to a volume of 5 mL with methanol. The EE and DL were determined by quantifying the total drug amount and the quantity of free drug in the supernatant using the chromatographic conditions as described in Section 2.4.1.

$$\text{EE (\%)} = (\text{total drug volume} - \text{free drug volume})/\text{total drug volume} \times 100\%$$

$$\text{DL (\%)} = (\text{total drug amount} - \text{free drug amount})/(\text{total drug amount} + \text{phospholipid amount}) \times 100\%$$

2.4 Method validation for FNB-Lip *in vitro*

2.4.1 Determination of maximum absorption wavelength. The detection wavelength of FNB (10 μg mL^{-1}) was determined using an Agilent 1260 Infinity HPLC system. The analytical conditions were as follows: an Agilent TC-C18 column (4.6 × 250 mm, 5 μm), methanol–water (90 : 10) used as the mobile phase, a flow rate set at 1.0 mL min^{-1}, a column temperature maintained at 30 °C, and an injection volume of 10 μL.

2.4.2 Specificity, precision, accuracy and stability analysis. The chromatographic peak positions of the blank solution (methanol), liposome solution (Lip), FNB standard solution (10 μg mL^{-1}), and FNB-Lip solution were observed according to the chromatographic conditions described in Section 2.4.1 to investigate the specificity of the analysis method. Additionally, a standard curve was generated by plotting the concentrations of FNB standard solutions (0, 2.0, 5.0, 10.0, 20.0, 40.0, 60.0, 80.0, 100.0 and 200.0 μg mL^{-1}) on the *x*-axis and their corresponding peak areas on the *y*-axis. Simultaneously, the peak areas of FNB-Lip solution at concentrations of 10, 20, and 40 μg mL^{-1} were measured to determine intra-day, inter-day precision and

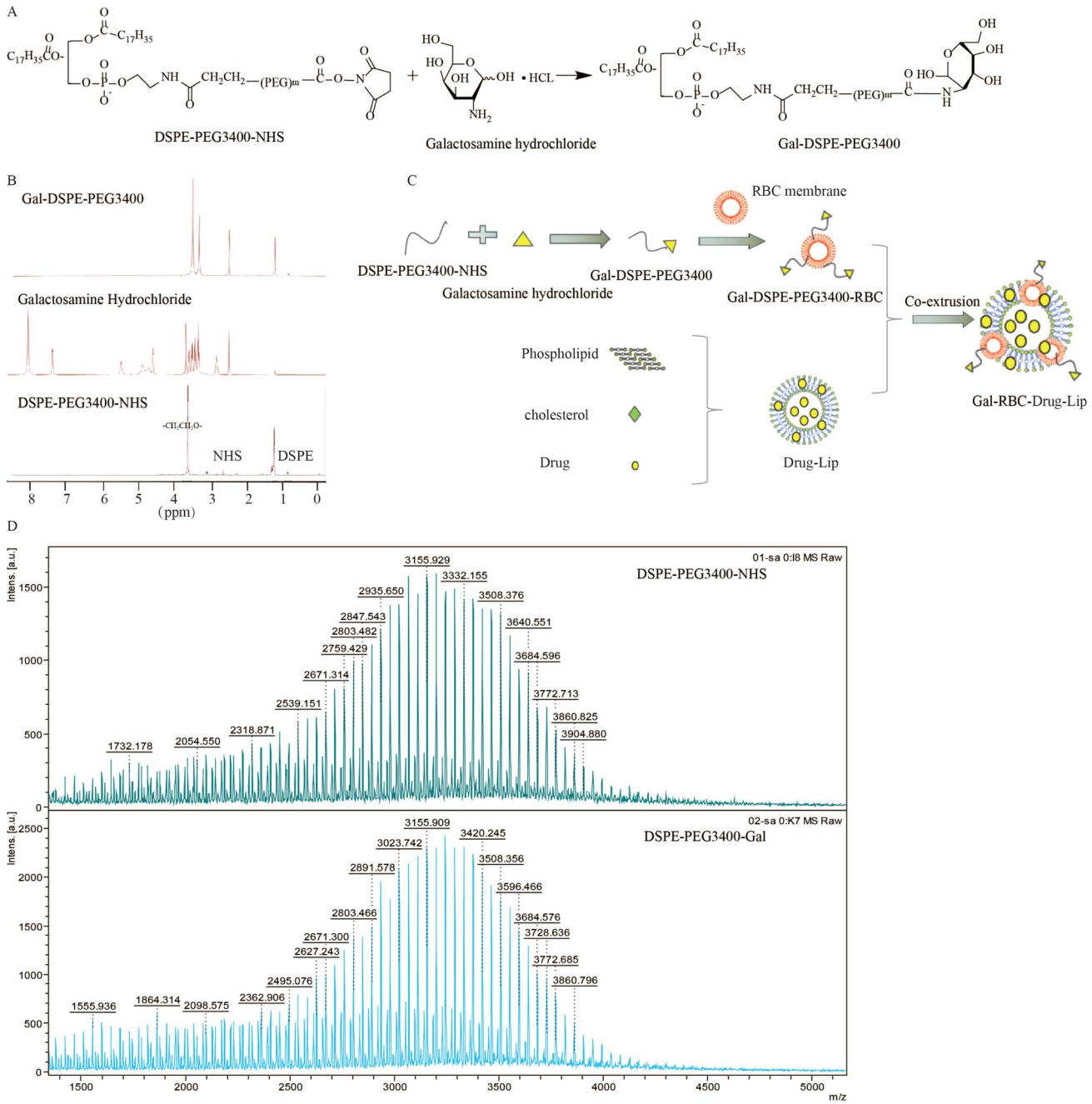

Fig. 1 Preparation of Gal-RBC-FNB-Lip. (A) Synthesis of Gal-DSPE-PEG3400. (B) ^{1}H-NMR. (C) Synthesis of Gal-RBC-FNB-Lip. (D) MALDI-TOF.

recovery rate. Additionally, the relative standard deviation (RSD) value of the FNB-Lip peak area within 48 h (0, 2, 4, 12, 24, and 48 h) was determined to evaluate its stability.

2.5 Preparation of galactose-modified erythrocyte membrane fusion liposome nanoparticles (Gal-RBC-FNB-Lip)

The DSPE-PEG3400-NHS was dissolved in anhydrous *N*,*N*-dimethylformamide (DMF), followed by the addition of triethylamine (TEA). After 12 h of sonication, galactosamine hydrochloride was introduced (DSPE-PEG3400-NHS : Gal : TEA = 1 : 2 : 1.2). Finally, the targeted material Gal-DSPE-PEG3400 was obtained through dialysis using a dialysis bag and subsequent freeze-drying (Fig. 1A). The structure of Gal-DSPE-PEG3400 was confirmed by ^{1}H-NMR analysis, as depicted in (Fig. 1B), where distinct proton chemical shift peaks corresponding to galactose (3.35 ppm) and DSPE (0.92 ppm) were observed for Gal-DSPE-PEG3400. Notably, no NHS signal was detected for targeting vector Gal-DSPE-PEG3400, indicating the successful synthesis. DSPE-PEG3400-NHS was a lipid molecule with an NHS (*N*-hydroxysuccinimide) active group. DSPE-PEG3400-Gal modified the end of the PEG chain by chemically introducing galactose (Gal) at the position of the NHS group. According to the MALDI-TOF analysis, there were certain differences in the main peak positions and characteristics of the two compounds, particularly in the high mass region. Specifically, the mass difference between peaks corresponding to the same PEG chain length has increased by approximately 162 Da. This indicates that galactose has been successfully connected at the end of the DSPE-PEG3400 molecule (Fig. 1D).

Then Gal-DSPE-PEG3400 was dissolved in 1× PBS erythrocyte membrane solution. Subsequently, the mixture was incubated in the dark for 2 h and then centrifuged to remove the supernatant, resulting in the formation of galactose-modified erythrocyte membrane (Gal-DSPE-PEG3400-RBC). After fragmentation, Gal-DSPE-PEG3400-RBC was added to the FNB-Lip solution. Finally, liposome extrusion was performed using a liposome extruder (HandExtruder™-1ml, Genizer Instruments Inc., USA) for 20 cycles followed by an additional 10 cycles through a polycarbonate film extrusion process to obtain galactose-modified erythrocyte membrane-fused fenofibrate liposomes (Gal-RBC-FNB-Lip) (Fig. 1C).

2.6 Morphological characterization and stability assessment of FNB-Lip and Gal-RBC-FNB-Lip

The FNB-Lip or Gal-RBC-FNB-Lip solution was diluted 10-fold with deionized water and subsequently deposited onto a copper net coated with a carbon film. After natural drying, the surface morphology of the sample was examined using transmission electron microscopy (TEM) (H-7650, Hitachi High-Technologies Corporation, China). At the same time, the targeted liposomes were diluted with 1× PBS and stored at 4 °C for evaluation of their stability by measuring particle size and polydispersity index (PDI) at 0, 7, 14, and 30 days.

The particle size and zeta potential of both FNB-Lip and Gal-RBC-FNB-Lip were determined in triplicate using a Malvern Zetasizer Nano ZS90 analyzer (Malvern Panalytical, UK) through dynamic light scattering (DLS) and electrophoretic light scattering (ELS) techniques, respectively. To investigate Förster resonance energy transfer (FRET), DiI and DiD were used for dual-labeling of the liposomes, with DiI serving as the fluorescence donor and DiD as the acceptor. The labeled liposomes (FNB-Lip) were then separated from unbound dyes and subsequently fused with Gal-RBC to form Gal-RBC-FNB-Lip. Fluorescence spectra of both FNB-Lip and Gal-RBC-FNB-Lip were recorded in the range of 550–750 nm.

2.7 *In vitro* release assay of Gal-RBC-FNB-Lip

The cumulative release percentage of Gal-RBC-FNB-Lip was determined by dialysis, with the FNB suspension used as a control. Specifically, 1 mL of Gal-RBC-FNB-Lip, Gal-FNB-Lip, RBC-FNB-Lip or FNB suspension was placed in a dialysis bag and subsequently immersed in 100 mL of release medium. At 0.5, 1, 2, 4, 8, 12, 24 and 48 h, aliquots (1 mL) of the release medium were withdrawn and subsequently mixed with an equal volume of fresh medium for subsequent measurement of FNB concentration. The cumulative release percentage was calculated using the following formula:

$$\left[\frac{C_n}{\frac{L}{V_2}} + \frac{\frac{(C_{n-1} + \ldots + C_2 + C_1)}{\frac{L}{V_2}} \times V_1}{V_2}\right] \times 100\%$$

2.8 Method validation for FNB acid *in vivo*

2.8.1 Chromatographic condition for FNB acid. The chromatography was conducted using a Diamonsil Diamond C18 column (250 mm × 4.6 mm, 5 μm) with a mobile phase consisting of methanol–water (80 : 20) at a flow rate of 1 mL min^{-1}. The column temperature was maintained at 30 °C, the sample volume injected was 20 μL, and the detection wavelength employed was set at 286 nm.

2.8.2 Specificity, precision, accuracy and stability analysis of plasma FNB acid. The FNB acid was dissolved in 10 mL of methanol to achieve a concentration of 1 mg mL^{-1} for the FNB mother liquor, and subsequently diluted with methanol to prepare the required FNB acid standard solution. The HPLC chromatographic peaks were then determined for the blank solvent, blank plasma sample, FNB acid standard solution, and FNB acid plasma sample to investigate the specificity of the analysis method. Additionally, a standard curve was generated by plotting the concentrations of FNB standard solutions (0, 1, 2, 3, 4, 5, 6, 7, 8, 9 and 10 μg mL^{-1}) on the *x*-axis against their corresponding peak areas on the *y*-axis. Furthermore, the peak areas of FNB acid plasma samples (1, 2 and 4 μg mL^{-1}) were measured to determine intra-day precision, inter-day precision and recovery rate. Simultaneously, the stability was evaluated after FNB acid (100, 4000, and 20 000 ng mL^{-1}) was stored at room temperature for 24 hours or subjected to repeated freeze-thaw cycles.

2.9 The absorption of Gal-RBC-FNB-Lip *in vivo*

Thirty healthy male ICR mice weighing 19 ± 1 g were randomly allocated into six groups, namely FNB (10, 20, 40 mg kg^{-1}), Gal-FNB-Lip (10, 20, 40 mg kg^{-1}), RBC-FNB-Lip (10, 20, 40 mg kg^{-1}) and Gal-RBC-FNB-Lip (10, 20, 40 mg kg^{-1}), with five mice per group. After a period of 12 h, blood samples were collected from the orbital socket to determine the concentration of FNB acid. The animal experiments were conducted in compliance with the legislation governing the utilization and welfare of laboratory animals in China and were approved by the Animal Ethics Committee of Shanxi Medical University (No. 22829).

2.10 Antilipemic effect of Gal-RBC-FNB-Lip on *in vitro* models of lipid deposition cells

The HL-02 cells in the logarithmic growth phase were seeded at a density of 1×10^5 cells per mL in culture dishes and treated with FNB (0.5 μmol L^{-1}, 1 μmol L^{-1}), Gal-FNB-Lip (0.5 μmol L^{-1}, 1 μmol L^{-1}), RBC-FNB-Lip (0.5 μmol L^{-1}, 1 μmol L^{-1}) or Gal-RBC-FNB-Lip (0.5 μmol L^{-1}, 1 μmol L^{-1}) for 24 h. Subsequently, the cells were subjected to a 24 h intervention with 5% palmitic acid before TC and TG levels were detected at 510 nm.

2.11 Targeting of Gal-RBC-FNB-Lip to hepatocytes

According to the preparation method of FNB-Lip and Gal-RBC-FNB-Lip, rhodamine B liposome nanoparticles (RhB-Lip) and galactose-modified erythrocyte membrane fusion rhodamine B liposome nanoparticles (Gal-RBC-RhB-Lip) were prepared and characterized using transmission electron microscopy (TEM). HL-02 cells in the logarithmic growth phase were seeded in 6-well plates and subsequently incubated with three rhodamine B fluorescent probes (RhB, RhB-Lip, Gal-RhB-Lip, Gal-RBC-RhB-Lip) for 2 h. Finally, the cells were washed with PBS and observed under a fluorescence microscope (Olympus IX-51, Tokyo, Japan).

2.12 Targeting of Gal-RBC-FNB-Lip to mice liver

According to the preparation methods of FNB-Lip and Gal-RBC-FNB-Lip, Indocyanine green liposome nanoparticle (ICG-Lip) and galactose-modified red cell membrane fusion indocyanine green liposome nanoparticle (Gal-RBC-ICG-Lip) were synthesized. Subsequently, mice were depilated and randomly divided into four groups with three mice per group. They were then intravenously injected with ICG, ICG-Lip, Gal-ICG-Lip and Gal-RBC-ICG-Lip (100 μL/10 g). At 0 min, 10 min, 1 h, 2 h, 4 h, 8 h, 12 h, and 24 h post-injection, the mice were placed in a small animal *in vivo* imager to visualize the distribution and fluorescence intensity using an excitation wavelength of 780 nm and an emission wavelength of 845 nm. Finally, the mice were euthanized for subsequent analysis by dissecting their heart, liver, spleen, lung, and kidney to evaluate fluorescence intensity.

2.13 Data statistics and analysis

The statistical analysis of all data was conducted using SPSS 23.0 software. A *t*-test was employed for intergroup comparisons, with statistical significance determined at a P value less than 0.05.

3. Results

3.1 Preparation, optimization and characterization of FNB-Lip

3.1.1 Preparation and optimization of FNB-Lip. The FNB-Lip samples were prepared using an orthogonal experimental design, and the encapsulation efficiency (EE) and drug loading (DL) of FNB were measured in (Table 3). Additionally, a homogeneity of variance test was conducted with phospholipid concentration, the ratio of phospholipid to cholesterol, and the ratio of phospholipid to drug as independent variables and EE and DL as dependent variables (Table 4). It was observed that

Table 3 Orthogonal experiment

	Factors				
Groups	Phospholipid concentration (mg mL^{-1})	Phospholipid–cholesterol ratio	Phospholipid–drug ratio	EE (%)	DL (%)
1	30	5 : 1	8 : 1	94.0	11.0
2	30	3 : 1	6 : 1	95.3	13.6
3	50	5 : 1	6 : 1	93.6	13.5
4	40	2 : 1	8 : 1	94.7	10.6
5	40	4 : 1	6 : 1	94.6	13.3
6	20	5 : 1	5 : 1	96.5	16.1
7	20	2 : 1	6 : 1	92.1	13.9
8	20	3 : 1	3 : 1	97.3	24.3
9	40	5 : 1	3 : 1	97.8	24.4
10	20	4 : 1	8 : 1	97.6	11.3
11	50	3 : 1	8 : 1	92.5	10.2
12	50	4 : 1	3 : 1	97.8	24.6
13	30	2 : 1	3 : 1	97.1	24.5
14	40	3 : 1	5 : 1	95.5	15.9
15	50	2 : 1	5 : 1	96.4	16.1
16	30	4 : 1	5 : 1	94.1	15.8

Table 4 Analysis of homogeneity for variance

Dependent variables	Independent variables	*F*	*P*
EE	Lipid concentration	0.181	0.906
	Phospholipid–cholesterol ratio	0.197	0.895
	Phospholipid–drug ratio	3.108	0.110
DL	Lipid concentration	1.088	0.423
	Phospholipid–cholesterol ratio	0.633	0.620
	Phospholipid–drug ratio	1631.713	0.000

except for when DL was considered as the dependent variable and the ratio of phospholipid to drug as the independent variable, the variances of the other groups were equivalent ($p > 0.05$). These findings suggested that DL was significantly affected by the ratio of phospholipid to drug, which was subsequently confirmed by LSD analysis (Table 5). Particularly, the ratios of 3 : 1 or 6 : 1 exhibited a pronounced impact on EE and DL (Table 5). Meanwhile, the response surface results also revealed a significant impact on DL when the lipid-drug ratio was 3 : 1, which was consistent with the findings from orthogonal experiments (Fig. 2). In summary, the optimal preparation conditions for FNB-Lip were determined to be a phospholipid : cholesterol : FNB ratio of 9 : 1 : 3.

3.1.2 Method validation for FNB-Lip *in vitro*

3.1.2.1 Determination of maximum absorption wavelength. The maximum absorption peak of the FNB standard solution (10 μg mL^{-1}) was observed at 288 ± 2 nm, confirming 288 nm as the optimal detection wavelength for FNB analysis (Fig. 3A).

3.1.2.2 Specificity, precision, accuracy and stability analysis of FNB-Lip. The peak time of the FNB-Lip solution (TR = 5.7 min) was found to be consistent with that of the FNB standard solution (Fig. 3B), thereby confirming excellent specificity. Additionally, a standard curve was generated with an R^2 value of

Table 5 LSD analysis for multiple comparisons[a,b]

Groups	(*I*)	(*J*)	*P*	
			EE as dependent variable	DL as dependent variable
Phospholipid concentration (mg mL^{-1})	20	30	0.558	0.398
		40	0.848	0.145
		50	0.583	0.209
	30	20	0.558	0.398
		40	0.689	0.473
		50	0.968	0.636
	40	20	0.848	0.145
		30	0.689	0.473
		50	0.717	0.798
	50	20	0.583	0.209
		30	0.968	0.636
		40	0.717	0.798
Phospholipid–cholesterol ratio	2	3	0.859	0.288
		4	0.488	0.871
		5	0.757	0.991
	3	2	0.859	0.288
		4	0.601	0.358
		5	0.895	0.283
	4	2	0.488	0.871
		3	0.601	0.358
		5	0.693	0.861
	5	2	0.757	0.991
		3	0.895	0.283
		4	0.693	0.861
Phospholipid–drug ratio	3	5	0.186	0.000*
		6	0.026*	0.000*
		8	0.075	0.000*
	5	3	0.186	0.000*
		6	0.199	0.000*
		8	0.535	0.000*
	6	3	0.026*	0.000*
		5	0.199	0.000*
		8	0.461	0.000*
	8	3	0.075	0.000*
		5	0.535	0.000*
		6	0.461	0.000*

[a] Lipid concentration: (*I*) and (*J*) were lipid concentrations; phospholipid–cholesterol ratio: (*I*) and (*J*) were phospholipid–cholesterol ratio; phospholipid–drug ratio: (*I*) and (*J*) were phospholipid–drug ratio. [b] * $p < 0.05$.

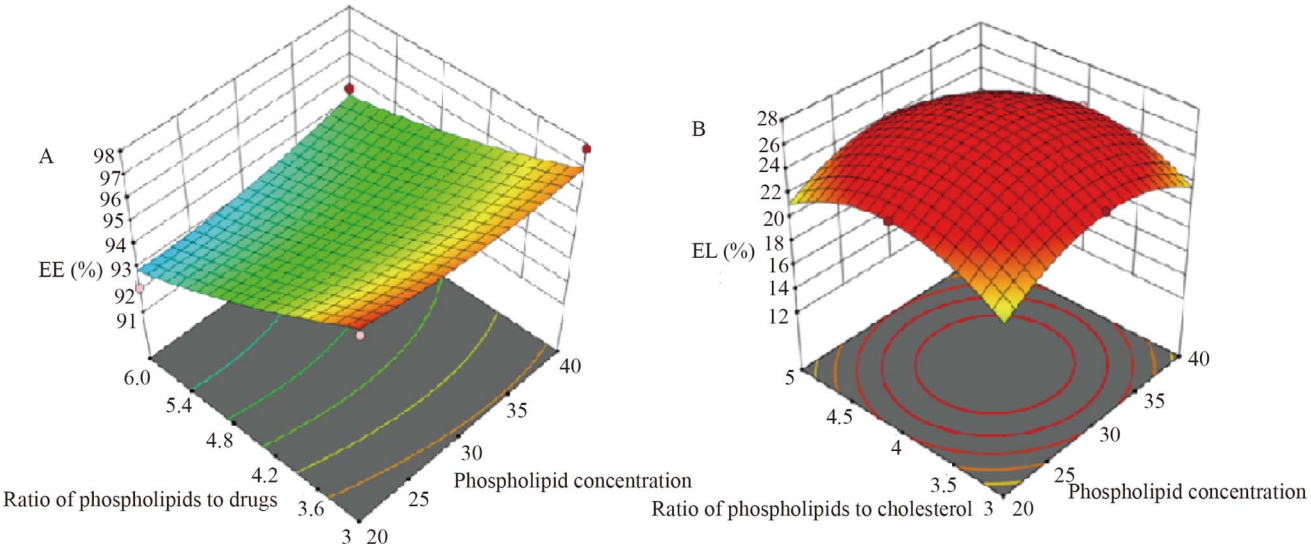

Fig. 2 The 3D response surface results. (A) EE. (B) DL.

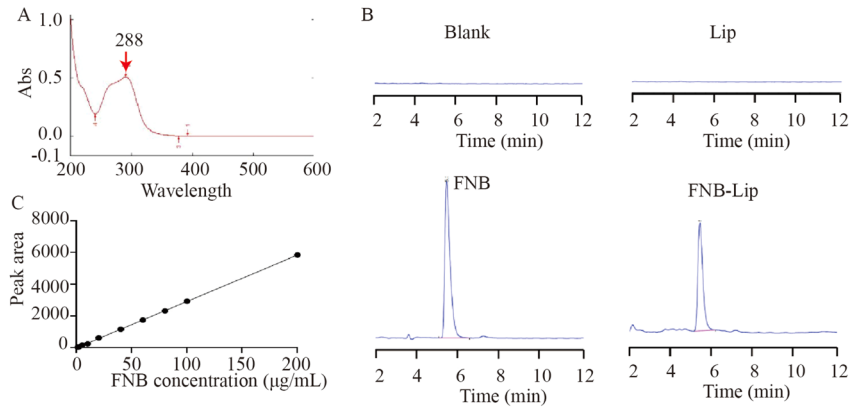

Fig. 3 Maximum absorption wavelength, specificity, and standard curve analysis. (A) Maximum absorption wavelength. (B) Specificity analysis. (C) Standard curve.

0.99 ($Y = 29.287X + 4.1113$) (Fig. 3C). At the same time, the relative standard deviation (RSD) value of the FNB-Lip peak area within 48 h was determined to be 0.2%, indicating excellent stability (Table 6). Furthermore, the RSD values for intra-day and inter-day precision of FNB-Lip were found to be less than 2.0% (Table 7), and the sample recovery rate ranged between 98.0% and 102.0% (Table 7). In a word, the specificity, precision, accuracy and stability were satisfactory for bioanalytical analysis.

Table 6 Stability test of FNB-Lip solution

Time (h)	Peak area (A)	Average value	RSD (%)
0	248.6	247.7 ± 0.60	0.2
2	248.2		
4	247.9		
12	247.5		
24	247.2		
48	247.1		

3.1.3 Characterization of FNB-Lip. According to the optimal preparation conditions (phospholipid : cholesterol : FNB = 9 : 1 : 3), the drug-loaded liposomes (FNB-Lip) were prepared. The EE, EL, particle size, and polydispersity index (PDI) were determined as 97.5 ± 0.2%, 24.7 ± 0.5%, 89.93 nm, and 0.263, respectively (Fig. 4A). Additionally, TEM analysis confirmed the spherical morphology of FNB-Lip, meeting the general requirements for liposome characterization (Fig. 4B). Subsequently, FNB-Lip was stored at 4 °C for 30 days to assess its stability by monitoring changes in particle size and PDI. Remarkably, no significant alterations were observed in either the particle size (~90 nm) or PDI (~0.26) during this storage period (Fig. 4C), indicating excellent stability of FNB-Lip.

3.2 Preparation and characterization of Gal-RBC-FNB-Lip

The Gal-RBC-FNB-Lip was prepared according to the protocol described in Section 2.5, and subsequently subjected to comprehensive characterization as outlined below. The TEM analysis in (Fig. 5A) revealed that Gal-RBC-FNB-Lip was either

Table 7 Precision and recovery test of FNB-Lip solution

Concentration ($\mu g\ mL^{-1}$)	Intra-day precision (%) ($n = 5$)	Inter-day precision (%) ($n = 15$)	Recovery rate (%) ($n = 3$)	RSD of recovery rate (%)
10	0.13	0.16	99.7	0.53
20	0.16	0.12	98.7	0.46
40	0.14	0.21	100.1	0.49

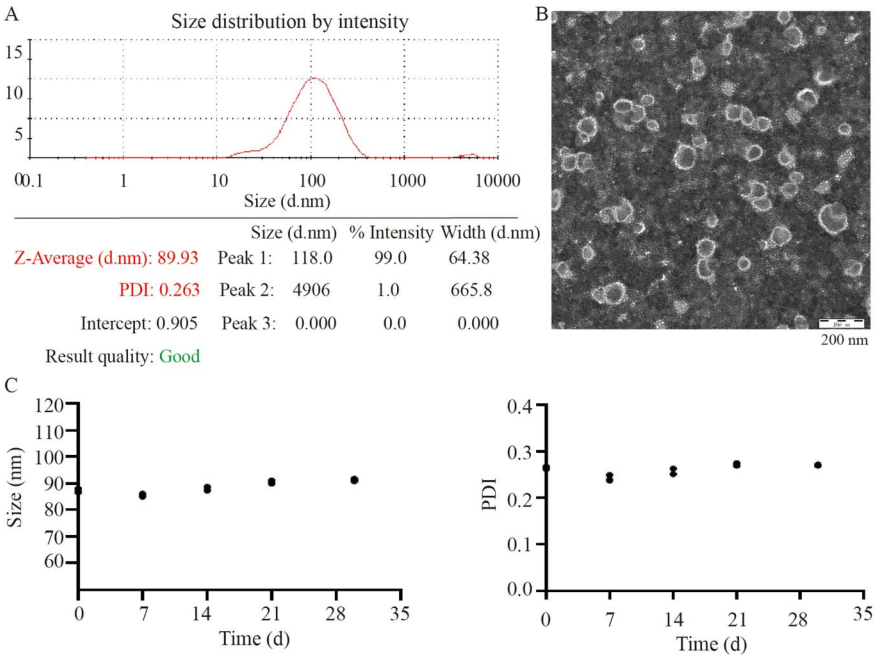

Fig. 4 Morphological examination and stability assessment of FNB-Lip. (A) Particle size analysis. (B) TEM image. (C) Placement stability analysis.

coated with a light-colored RBC membrane or completely fused with it. Moreover, it was observed that the particle size of Gal-RBC-FNB-Lip (97.4 nm) was larger than that of FNB-Lip (89.93 nm) (Fig. 5B).

As shown in (Fig. 5C) and (Table 8), the zeta potentials of RBC, FNB-Lip, and Gal-RBC-FNB-Lip were -18.4 ± 3.4 mV, -10.2 ± 1.5 mV, and -17.1 ± 2.3 mV, respectively. The negative zeta potentials were primarily attributed to the fusion of RBCs with the liposomes. Simultaneously, as depicted in (Fig. 5D), FRET analysis comparing the fluorescence spectra of FNB-Lip (pre-fusion) and Gal-RBC-FNB-Lip (post-fusion) revealed a substantial increase in fluorescence intensity at the donor DiI characteristic peak (565 nm), accompanied by a synchronous decrease at the acceptor DiD peak (665 nm) in Gal-RBC-FNB-Lip. These findings indicated a marked reduction in FRET efficiency, which was attributed to an increased intermolecular distance between the fluorescent donor and acceptor, confirming successful membrane fusion between FNB-Lip and Gal-RBC.

The particle sizes of FNB-Lip and Gal-RBC-FNB-Lip were summarized in (Table 8). The average particle size of FNB-Lip was approximately 89.93 ± 1.5 nm, and the PDI was 0.254 ± 0.01. For Gal-RBC-FNB-Lip, the particle size was 97.4 ± 2.1 nm, and the PDI was 0.26 ± 0.02. The size distribution results indicated that both FNB-Lip and Gal-RBC-FNB-Lip exhibited uniformity. Furthermore, after 30 days at 4 °C, the particle size of Gal-RBC-FNB-Lip remained stable at approximately 95 nm and exhibited a PDI range of 0.26–0.27 indicating excellent stability (Fig. 5E).

3.3 Pharmacodynamics study for Gal-RBC-FNB-Lip

3.3.1 Specificity, precision, accuracy and stability analysis of plasma FNB acid. HPLC analysis was performed for the blank solvent, blank plasma sample, FNB acid standard solution, and FNB acid plasma sample. The main peak time of plasma FNB acid was approximately 8.1 min, as shown in (Fig. 6A). This was consistent with the peak time of the FNB acid standard solution. Additionally, a standard curve was generated with an R^2 value of 0.99 ($Y = 61.314X - 4.1763$) (Fig. 6B). The RSD values for intra-day and inter-day precision of FNB-Lip were found to be less than or equal to 2.0% (Table 9) and the sample recovery rate ranged from 95.0% to 101.0% (Table 9). Additionally, the stability study showed that the content of FNB acid remained stable when the sample was stored at room temperature for 24 h or subjected to repeated freeze-thaw cycles (Table 10). In

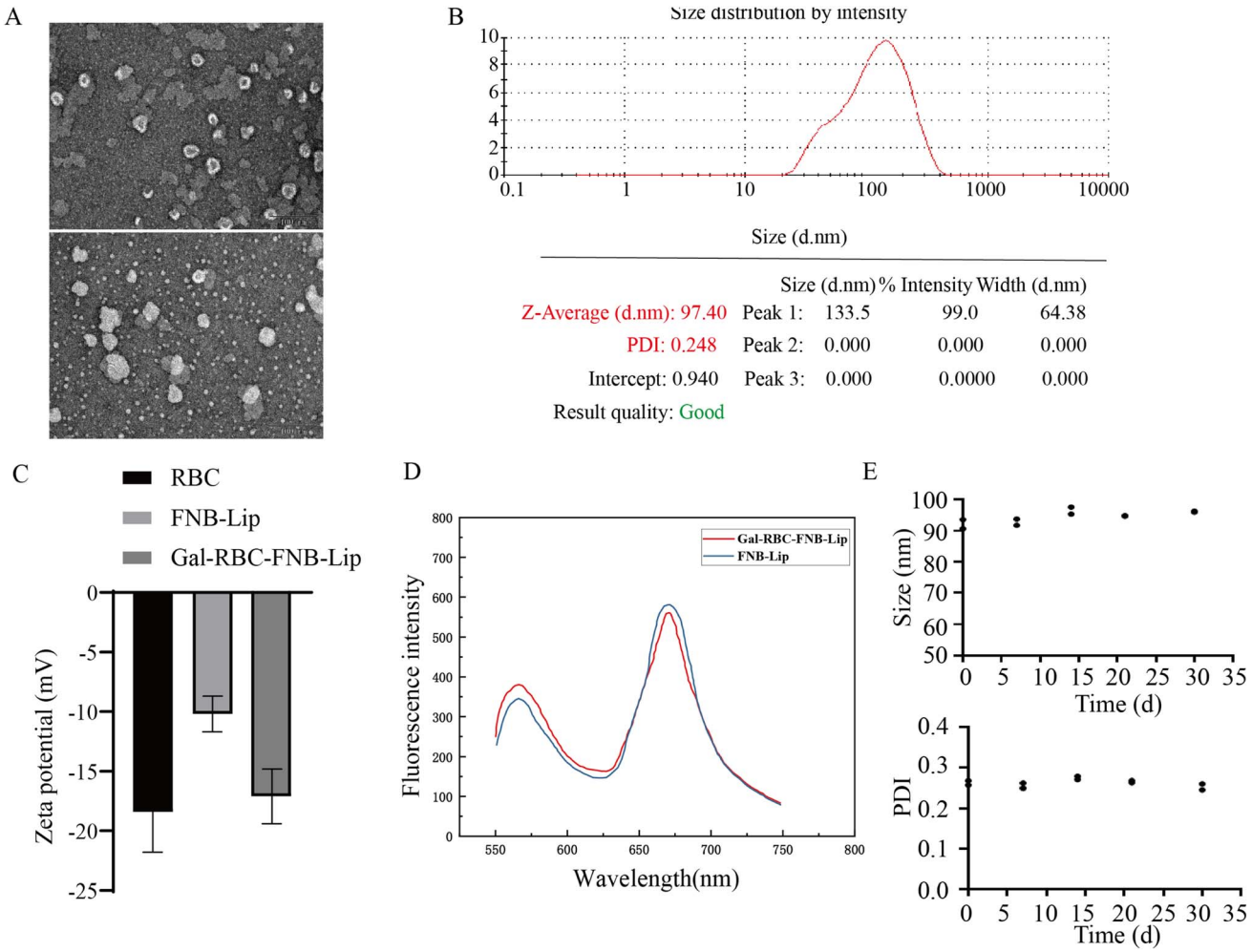

Fig. 5 Characterization of Gal-RBC-FNB-Lip. (A) TEM analysis of Gal-RBC-FNB-Lip. (B) Size analysis of Gal-RBC-FNB-Lip. (C) Zeta potentials of RBC, FNB-Lip, and Gal-RBC-FNB-Lip. (D) FRET fusion images. (E) Stability analysis of Gal-RBC-FNB-Lip.

Table 8 Sizes and zeta potentials of RBC, FNB-Lip, and Gal-RBC-FNB-Lip

Group	Zeta potential (mV)	Mean size (nm)	Polydispersity index (PDI)
RBC	−18.4 ± 3.4	—	—
FNB-Lip	−10.2 ± 1.5	89.93 ± 1.5	0.254 ± 0.01
Gal-RBC-FNB-Lip	−17.1 ± 2.3	97.4 ± 2.1	0.26 ± 0.02

summary, the specificity, precision, accuracy and stability were satisfactory for bioanalytical analysis.

3.3.2 Antilipemic effect of Gal-RBC-FNB-Lip. *In vitro* release experiments (Fig. 7A) showed that the cumulative release of FNB reached 85%, Gal-FNB-Lip reached 77%, and RBC-FNB-Lip reached 73% within 48 h, while Gal-RBC-FNB-Lip exhibited a delayed release profile with only 38%, highlighting its ability to prolong drug release. The *in vivo* absorption experiments revealed that the blood concentration of FNB acid in the Gal-RBC-FNB-Lip group was significantly higher than that in the FNB group, while there was no significant difference between Gal-FNB-Lip group and RBC-FNB-Lip group, indicating that even at lower concentrations, Gal-RBC-FNB-Lip could achieve therapeutic efficacy equivalent to higher concentrations of FNB (Fig. 7B). Additionally, all four groups exhibited the ability to decrease TC and TG levels, with no statistically significant difference in HL-02 cells (Fig. 7C). These results demonstrated that, in comparison to FNB, Gal-RBC-FNB-Lip exhibited a sustained release effect. Furthermore, it could effectively enhance the blood drug concentration of FNB acid while preserving the lipid-lowering effect of FNB.

3.4 Liver-targeting efficacy of galactose-modified erythrocyte membrane fusion liposomes

Following the previously described synthesis process, a RhB-labeled fluorescent liposome was prepared to investigate its targeting effect on HL-02 cells. As depicted in (Fig. 8A), similar to Gal-RBC-FNB-Lip, Gal-RBC-RhB-Lip also exhibited two distinct fusion conditions, confirming the occurrence of dual fusion phenomena during the preparation of red cell membrane-fused liposomes *via* liposomal co-extrusion.

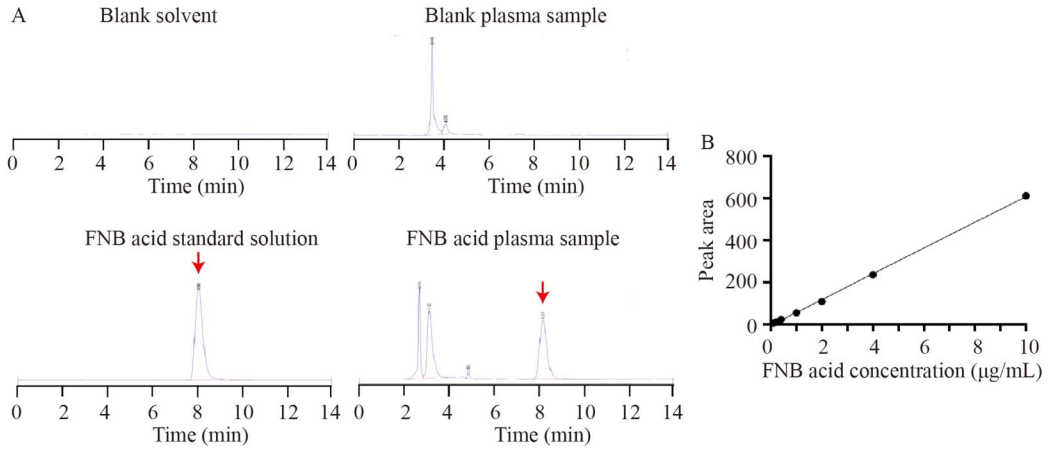

Fig. 6 HPLC detection and construction of the standard curve. (A) HPLC detection. (B) Construction of the standard curve.

Table 9 Precision and recovery test of FNB acid plasma samples

Concentration (μg mL^{-1})	Intra-day precision (%) (n = 5)	Inter-day precision (%) (n = 15)	Recovery rate (%) (n = 3)	RSD (%)
1	1.73	1.69	95.5	1.50
2	1.49	1.41	97.4	1.36
4	1.65	1.75	100.1	1.72

Table 10 Stability of FNB acid in biological samples

Under circumstances	Concentration (ng mL^{-1})	Measured quantity (ng mL^{-1})	SD	RSD (%)
After 24 h at room temperature (n = 5)	100	97.1	3.5	3.6
	4000	4066.6	20.3	0.5
	20 000	20 633.3	235.2	1.14
After repeated freeze-thaw (−20 °C, 3 days) (n = 5)	100	90.5	4.7	5.3
	4000	4120.7	16.5	0.4
	20 000	20 416.6	285.8	1.4

Furthermore, it was observed that Gal-RBC-RhB-Lip had a particle size of approximately 91.35 nm and a PDI range between 0.26 and 0.27 (Fig. 8B). After a 2 h incubation of RhB, RhB Lip, Gal-RhB-Lip and Gal-RBC-RhB-Lip, as depicted in (Fig. 8C), a significant increase in the average fluorescence intensity was specifically observed in the Gal-RhB-Lip and Gal-RBC-RhB-Lip group compared to the other two groups, indicating that Gal-RhB-Lip and Gal-RBC-RhB-Lip exhibited targeted potential towards hepatic cells.

Subsequently, ICG-labeled liposomes were prepared, and the targeted organ distribution of Gal-RBC-ICG-Lip in animals was investigated using an *in vivo* imaging system for small animals. As illustrated in (Fig. 8D), ICG was initially distributed systemically and subsequently exhibited gradual accumulation in the abdominal region, followed by subsequent metabolism in mice. Interestingly, ICG exhibited a remarkably rapid metabolic rate, while ICG-Lip and Gal-ICG-Lip displayed a slightly slower metabolism. Notably, Gal-RBC-ICG-Lip showed promising potential in significantly prolonging the *in vivo* metabolic process of ICG. Subsequently, the mouse isolated organs were placed in the *in vivo* imaging system. As depicted in (Fig. 8E), minimal residual fluorescence was observed in the ICG group, indicating substantial metabolic clearance of ICG. In the ICG-Lip group, a significant amount of fluorescence was detected in the liver, kidney, spleen, and lung, suggesting that ICG-Lip exhibited limited hepatic targeting specificity. However, upon administration of Gal-RBC-ICG-Lip to mice, the fluorescence was primarily observed in both the liver and kidney; notably with significantly higher intensity within the liver compared to that within the kidney. These findings indicated that Gal-RBC-ICG-Lip possessed precise targeting capabilities for drug delivery to liver tissue while minimizing drug absorption by other vital organs such as the heart, spleen, lung, and kidney.

4. Discussions

Liver diseases imposed a substantial global health burden, with an estimated 800 million cases and causing over 2 million

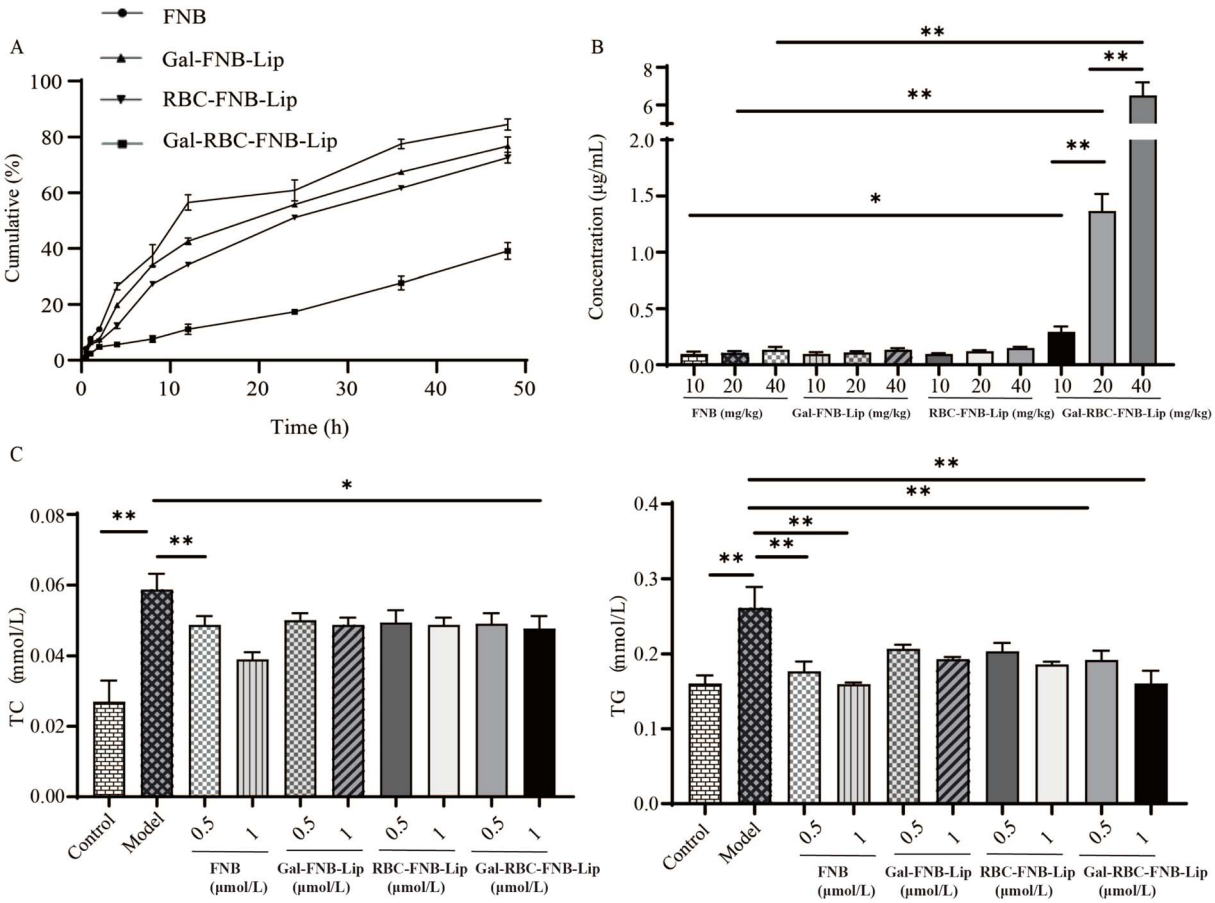

Fig. 7 Pharmacodynamics study for Gal-RBC-FNB-Lip. (A) Cumulative release assay *in vitro*. (B) Absorption experiments *in vivo*. (C) Antilipemic effect of Gal-RBC-FNB-Lip.

deaths annually worldwide.[28] The proportion of mortality attributed to liver diseases has consistently increased from 3% to 3.5% of the total global mortality in the past two decades.[29] The primary cause of liver disease in Africa and East Asia continued to be viral hepatitis, while Western industrialized countries were witnessing a rise in alcohol-related and non-alcoholic fatty liver disease.[30] In advanced stages of liver diseases, where curative options are limited, liver resection and transplantation remain the most successful treatments.[30] The major limitations of standard pharmacological therapies lied in their inability to achieve a therapeutic agent concentration sufficient for effective treatment of the diseased liver, as well as their tendency to induce undesirable systemic effects.[30] Consequently, there was a high demand for modern chemotherapies that offer enhanced stability of therapeutic agents and enable selective targeting specifically towards the afflicted liver cells.

Nanomedicine, which consists of a therapeutic drug formulated in a carrier with a typical size range of 10–200 nm, exhibited significant potential for addressing clinical challenges in the treatment of liver diseases.[31] These carriers commonly comprise biomacromolecules such as proteins, inorganic materials, polymers, and liposomes.[30] Among them, liposomes played a pivotal role as one of the most crucial carriers in targeted drug delivery systems. In this research, the synthesis of FNB-liposome was achieved by employing phospholipid, cholesterol, and FNB as initial materials and the optimal conditions for the preparation process were determined through an orthogonal experimental design. Additionally, to improve its targeting effect, the polymer Gal-DSPE-PEG3400 was inserted on its surface. It was noting that galactosamine (Gal) was a well-characterized hepatocytes-targeting moiety due to its specific binding with asialoglycoprotein receptor (ASGPR) on the surface of hepatocytes.[32] For instance, Chen *et al.* reported that the nanoparticle-siRNA system modified by Gal demonstrated enhanced gene silencing effects in hepatocytes compared to free siRNA and naked nanoparticles.[33] Additionally, the conjugation of antisense oligonucleotide and siRNA to Gal significantly facilitated their entry into hepatocytes.[34] In this study, Gal as ligands were conjugated to DSPE-PEG3400-RBC and liposoluble DSPE molecule embedded in the liposome bilayer, while the water-soluble component of sugar exposed on the surface of liposome. Then, Gal could efficiently deliver drugs such as FNB to the specific tissue (liver) after binding to the related receptor (ASGPR). Through *in vivo* and *in vitro* experiments, this study demonstrated that the Gal-PEG-DSPE-RBC-FNB-LiP delivery system offered several

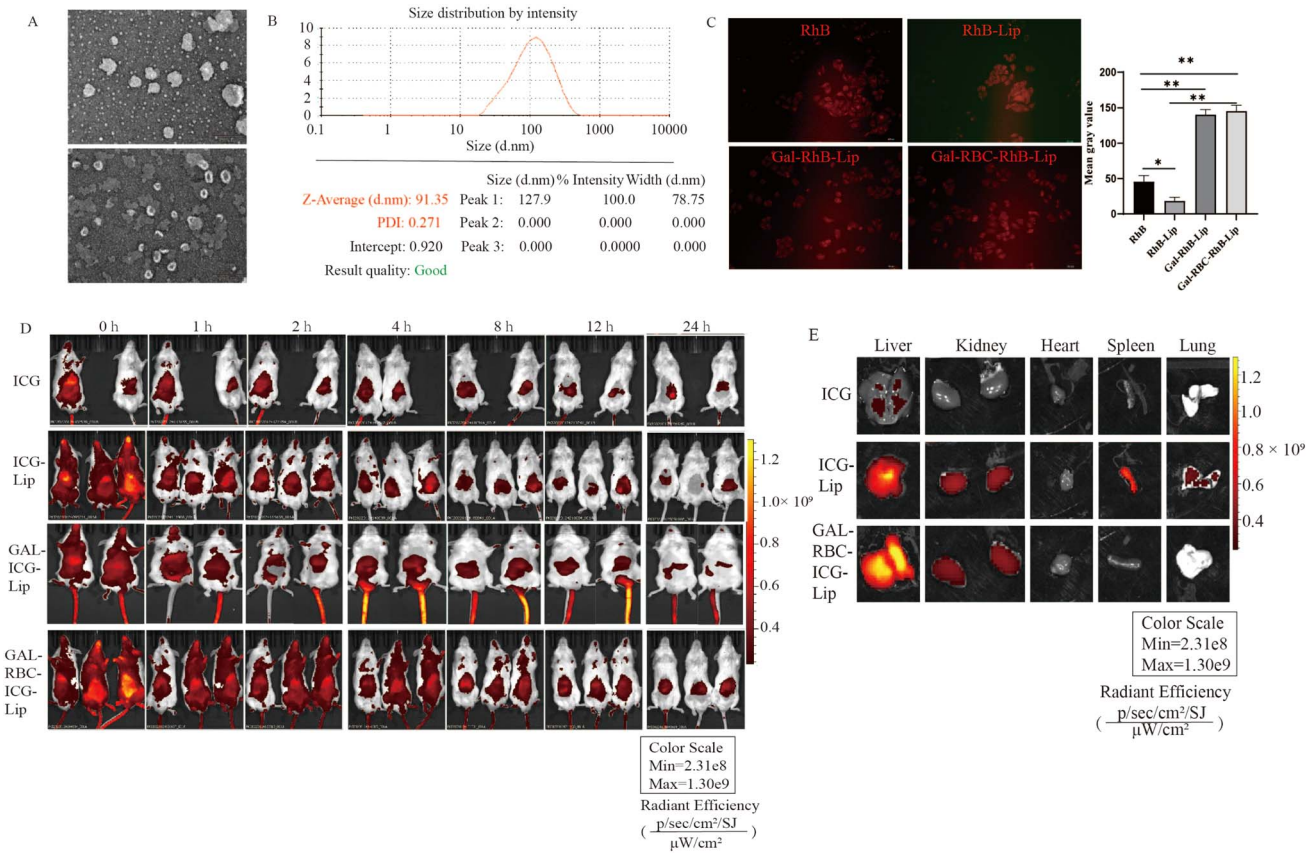

Fig. 8 The liver-targeting efficacy of galactose-modified erythrocyte membrane fusion liposomes. (A) The TEM of Gal-RBC-RhB-Lip. (B) The particle size of Gal-RBC-RhB-Lip. (C) The fluorescence in HL-02 cells after administration of RhB-Lip, Gal-RhB-Lip and Gal-RBC-RhB-Lip. (D) The fluorescence of ICR mice after tail vein injection of ICG, ICG-Lip, Gal-ICG-Lip and Gal-RBC-ICG-Lip. (E) The fluorescence of isolated organs (*$p < 0.05$, **$p < 0.01$).

advantages over free FNB. Not only did it preserve the therapeutic efficacy of drugs, but it also effectively stabilized drug release rates and prolonged drug release duration, thereby exhibiting a distinct advantage in achieving prolonged circulation. At the same time, it might also be more accurately targeted to the liver site, thereby improving the effectiveness of treatment and reducing the possibility of toxic effects of drug absorption by other tissues and organs.

5. Conclusions

In summary, liver-targeted Gal-RBC-FNB-Lip was successfully prepared using a lipid co-extrusion technique. By utilizing lipid tethers and the flexible structure of membrane bilayers, liver-targeting ligands (Gal-DSPE-PEG3400-RBC) could be seamlessly integrated onto the FNB-Lip platform without requiring chemical reactions. Importantly, this study demonstrated significant potential for liver targeted therapy with Gal-RBC-FNB-Lip, which not only exhibited specific targeting towards liver cells but also possessed desirable characteristics such as biocompatibility, extended circulation time, and reduced toxicity. Therefore, the simplicity and robustness of this functionalization approach might facilitate the development of Gal-RBC-FNB-Lip for targeted therapy against hepatic disorders.

Data availability

The authors confirm that the data supporting the findings of this study are available within the article. Data are available from the corresponding author.

Author contributions

Jiayu Song wrote the manuscript. Yan Sun and Yuan Ren helped perform the experiments. Dan Peng, Meiying Liu and Xiaohui Zhang analyzed the data. Huanhuan Zhang and Xiaohui Zhang commented and corrected the paper. Yunlan Li was responsible for supervision.

Conflicts of interest

None of the authors has a conflict of interest to declare.

Abbreviations

RBC	red blood cell
FNB-Lip	fenofibrate liposome nanoparticles

Gal-RBC-FNB-Lip	galactose-modified erythrocyte membrane fusion liposome nanoparticles
ASGPR	sialic acid glycoprotein receptor
FNB	fenofibrate
EE	encapsulation efficiency
DL	drug loading
PDI	polydispersity index
ICG-Lip	indocyanine green liposome nanoparticles
Gal-RBC-ICG-Lip	galactose-modified red cell membrane fusion indocyanine green liposome nanoparticles
TEM	transmission electron microscopy
Gal	galactosamine
RhB-Lips	rhodamine B liposome nanoparticles
Gal-RBC-RhB-Lips	galactose-modified erythrocyte membrane fusion rhodamine B liposome nanoparticles
FRET	Förster resonance energy transfer

Acknowledgements

This work was supported by grants from the National Natural Science Foundation (81973411, China); the Scientific Research Funding Project for Returned Students in Shanxi Province (2020-084, China); the Key Research and Development Project of Shaanxi Province (2023-YBSF-225, China); the Shanxi Key Laboratory of Food and Drug Safety Open Subject "Study on the processing technology and safety evaluation of keel"; the Shaanxi Provincial Administration of Traditional Chinese Medicine; the 2023 Double First-Class Creation Action Project (2C622023009); the Key Laboratory of Coal Environmental Pathogenicity and Prevention (Shanxi Medical University) Ministry of Education (China); the Graduate Education Innovation program of Shanxi Province (2024KY362); the Shanxi Medical University Double First-class to create action Innovative drug Research and development project (IDD/SXMU-2024-01); Luohe City Innovative Science and Technology Team (China); the Science and Technology Research Project of Henan Province (252102310430).

References

1 H. Devarbhavi, S. K. Asrani, J. P. Arab, *et al.*, Global burden of liver disease: 2023 update, *J. Hepatol.*, 2023, **79**(2), 516–537.
2 B. Baran and F. Akyuz, Non-alcoholic fatty liver disease: what has changed in the treatment since the beginning?, *World J. Gastroenterol.*, 2014, **20**(39), 14219–14229.
3 Q. Long, F. Luo, B. Li, *et al.*, Gut microbiota and metabolic biomarkers in metabolic dysfunction-associated steatotic liver disease, *Hepatol. Commun.*, 2024, **8**(3), e0310.
4 S. Bluemel, B. Williams, R. Knight, *et al.*, Precision medicine in alcoholic and nonalcoholic fatty liver disease via modulating the gut microbiota, *Am. J. Physiol.: Gastrointest. Liver Physiol.*, 2016, **311**(6), G1018–G1036.
5 R. L. Chen, Q. X. Wang and X. Ma, Precision medicine for autoimmune hepatitis, *J. Dig. Dis.*, 2019, **20**(7), 331–337.
6 M. R. Carvalho, R. L. Reis and J. M. Oliveira, Dendrimer nanoparticles for colorectal cancer applications, *J. Mater. Chem. B*, 2020, **8**(6), 1128–1138.
7 R. Vichare and J. M. Janjic, Macrophage-Targeted Nanomedicines for ARDS/ALI: Promise and Potential, *Inflammation*, 2022, **45**(6), 2124–2141.
8 C. Long, H. Peng, W. Yang, *et al.*, Targeted Delivery of Gemcitabine for Precision Therapy of Cholangiocarcinoma Using Hyaluronic Acid-Modified Metal-Organic Framework Nanoparticles, *ACS Omega*, 2024, **9**(10), 11998–12005.
9 J. Xu, S. Chen, J. Yang, *et al.*, Hyaluronidase-trigger nanocarriers for targeted delivery of anti-liver cancer compound, *RSC Adv.*, 2023, **13**(16), 11160–11170.
10 M. Monestier, P. Charbonnier, C. Gateau, *et al.*, ASGPR-Mediated Uptake of Multivalent Glycoconjugates for Drug Delivery in Hepatocytes, *Chembiochem*, 2016, **17**(7), 590–594.
11 Y. Zhang, X. Zhang, C. Zeng, *et al.*, Targeted delivery of atorvastatin via asialoglycoprotein receptor (ASGPR), *Bioorg. Med. Chem.*, 2019, **27**(11), 2187–2191.
12 D. Santo, R. A. Cordeiro, P. V. Mendonca, *et al.*, Glycopolymers Mediate Suicide Gene Therapy in ASGPR-Expressing Hepatocellular Carcinoma Cells in Tandem with Docetaxel, *Biomacromolecules*, 2023, **24**(3), 1274–1286.
13 E. Y. Yamansarov, E. V. Lopatukhina, S. A. Evteev, *et al.*, Discovery of Bivalent GalNAc-Conjugated Betulin as a Potent ASGPR-Directed Agent against Hepatocellular Carcinoma, *Bioconjugate Chem.*, 2021, **32**(4), 763–781.
14 A. A. D'Souza and P. V. Devarajan, Asialoglycoprotein receptor mediated hepatocyte targeting - strategies and applications, *J. Controlled Release*, 2015, **203**, 126–139.
15 Y. Liu, M. Tan, Y. Zhang, *et al.*, Targeted Gene Silencing BRAF Synergized Photothermal Effect Inhibits Hepatoma Cell Growth Using New GAL-GNR-siBRAF Nanosystem, *Nanoscale Res. Lett.*, 2020, **15**(1), 116.
16 A. Nagode, J. Vanbeselaere, Z. Dutkiewicz, *et al.*, Molecular characterisation of Entamoeba histolytica UDP-glucose 4-epimerase, an enzyme able to provide building blocks for cyst wall formation, *PLoS Neglected Trop. Dis.*, 2023, **17**(8), e11574.
17 M. Jurczyk, K. Jelonek, M. Musial-Kulik, *et al.*, Single- versus Dual-Targeted Nanoparticles with Folic Acid and Biotin for Anticancer Drug Delivery, *Pharmaceutics*, 2021, **13**(3).
18 J. Peng, S. Li and H. Ti, Sensitize Tumor Immunotherapy: Immunogenic Cell Death Inducing Nanosystems, *Int. J. Nanomed.*, 2024, **19**, 5895–5930.
19 B. Shaqour, A. Samaro, B. Verleije, *et al.*, Production of Drug Delivery Systems Using Fused Filament Fabrication: A Systematic Review, *Pharmaceutics*, 2020, **12**(6).
20 A. H. Faraji and P. Wipf, Nanoparticles in cellular drug delivery, *Bioorg. Med. Chem.*, 2009, **17**(8), 2950–2962.
21 X. Lang, X. Wang, M. Han, *et al.*, Nanoparticle-Mediated Synergistic Chemoimmunotherapy for Cancer Treatment, *Int. J. Nanomed.*, 2024, **19**, 4533–4568.
22 V. P. Chavda, L. V. Nalla, P. Balar, *et al.*, Advanced Phytochemical-Based Nanocarrier Systems for the Treatment of Breast Cancer, *Cancers*, 2023, **15**(4).
23 J. W. Yoo, D. J. Irvine, D. E. Discher, *et al.*, Bio-inspired, bioengineered and biomimetic drug delivery carriers, *Nat. Rev. Drug Discovery*, 2011, **10**(7), 521–535.

24 M. H. Rahman, C. Wong, M. M. Lee, *et al.*, Efficient encapsulation of functional proteins into erythrocytes by controlled shear-mediated membrane deformation, *Lab Chip*, 2021, **21**(11), 2121–2128.
25 S. Tan, T. Wu, D. Zhang, *et al.*, Cell or cell membrane-based drug delivery systems, *Theranostics*, 2015, **5**(8), 863–881.
26 A. A. Abulaban, H. M. Al-Kuraishy, A. I. Al-Gareeb, *et al.*, Role of fenofibrate in multiple sclerosis, *Eur. J. Med. Res.*, 2024, **29**(1), 113.
27 A. Pestieau, F. Krier, A. Brouwers, *et al.*, Selection of a discriminant and biorelevant in vitro dissolution test for the development of fenofibrate self-emulsifying lipid-based formulations, *Eur. J. Pharm. Sci.*, 2016, **92**, 212–219.
28 Y. Ren, Y. Chen, E. H. Tang, *et al.*, Arbidol attenuates liver fibrosis and activation of hepatic stellate cells by blocking TGF-beta1 signaling, *Eur. J. Pharmacol.*, 2024, **967**, 176367.
29 S. K. Asrani, H. Devarbhavi, J. Eaton, *et al.*, Burden of liver diseases in the world, *J. Hepatol.*, 2019, **70**(1), 151–171.
30 R. Bottger, G. Pauli, P. H. Chao, *et al.*, Lipid-based nanoparticle technologies for liver targeting, *Adv. Drug Delivery Rev.*, 2020, **154–155**, 79–101.
31 L. H. Reddy and P. Couvreur, Nanotechnology for therapy and imaging of liver diseases, *J. Hepatol.*, 2011, **55**(6), 1461–1466.
32 D. A. Wall and A. L. Hubbard, Galactose-specific recognition system of mammalian liver: receptor distribution on the hepatocyte cell surface, *J. Cell Biol.*, 1981, **90**(3), 687–696.
33 S. Chen, Y. Y. Tam, P. J. Lin, *et al.*, Development of lipid nanoparticle formulations of siRNA for hepatocyte gene silencing following subcutaneous administration, *J. Controlled Release*, 2014, **196**, 106–112.
34 A. D. Springer and S. F. Dowdy, GalNAc-siRNA Conjugates: Leading the Way for Delivery of RNAi Therapeutics, *Nucleic Acid Ther.*, 2018, **28**(3), 109–118.